

## A NUMERICAL STUDY OF A THREE-DIMENSIONAL PROTON EXCHANGE MEMBRANE FUEL CELL (PEMFC) WITH PARALLEL AND COUNTER FLOW GAS CHANNELS\*

N. AHMADI\*\*, H. TARAGHI AND M. SADEGHIAZAD

<sup>1</sup>Dept. of Mechanical Engineering, Urmia University of Technology, Urmia, I. R. of Iran  
Email: nima.ahmadi.eng@gmail.com

**Abstract**– Modeling the heat and mass transport in micro channel is being used extensively in researches and industrial applications. The aim is optimizing fuel cell designs before building a prototype for engineering application. In this study, numerical, three-dimensional, single phase computational fluid dynamics model of a proton exchange membrane fuel cell with both the gas distribution flow channels and the Membrane Electrode Assembly (MEA) has been developed. A single set of conservation equations which are valid for the flow channels, gas-diffusion electrodes, catalyst layers, and the membrane region, are solved by finite volume technique. The present simulated straight channels PEMFC model, accounts for major transport phenomena and the performance. Additionally, the effect of reversing the flow direction at cathode side has been investigated to study the fuel cell performance and species distribution. The results showed that, in the PEMFC with the counter flow channels, the output current density has been decreased and also the kind of species distributions has been influenced by this phenomenon. It is very important to model the back diffusion and electro-osmotic mass flux for determination of ionic conductivity of membrane which affects the performance of fuel cell. Finally, the numerical results are validated by available experimental data.

**Keywords**– PEM fuel cells, cell voltage, current density, counter flow, fuel cell performance

### 1. INTRODUCTION

Proton exchange membrane fuel cell (PEMFC) uses very thin polymer membrane as electrolyte. It has been considered as a promising candidate of future power sources, especially for transportation applications and residential power. This type of fuel cell has many important advantages such as high efficiency, clean, quiet, low temperature operation, capable of quick start-up, no liquid electrolyte and simple cell design. However, its performance and cost should be further optimized before this system becomes competitive with the traditional combustion power plants [1-3].

In recent years, research and development in fuel cells and fuel cell systems have been accelerated; but at present, the cost of fuel cell systems is still too high for them to become viable commercial products.

In a fuel cell, fuel (e.g., hydrogen gas) and an oxidant (e.g., oxygen gas from the air) are used to generate electricity, while heat and water are typical products of the fuel cell operation. A fuel cell typically works on the following principle: as the hydrogen gas flows into the fuel cell on the anode side, a platinum catalyst facilitates oxidation of the hydrogen gas which produces protons (hydrogen ions) and electrons. The hydrogen ions diffuse through a membrane (the center of the fuel cell which separates the anode and the cathode); and again with the help of a platinum catalyst, combine with oxygen and electrons

---

\*Received by the editors February 2, 2014; Accepted February 16, 2015.

\*\*Corresponding author

on the cathode side in order to produce water. The electrons, which cannot pass through the membrane, flow from the anode to the cathode through an external electrical circuit containing a motor or other electric system.

Both of the anode and cathode (the electrodes) are porous and made from an electrically conductive material, typically carbon. The electrode faces are in contact with the membrane which contains: carbon, polymer electrolyte and a platinum-based catalyst. The oxidation and reduction fuel-cell half reactions take place in the anode and the cathode active layer, respectively. The PEM electrodes are of gas-diffusion type and generally designed for maximum surface area per unit material volume (the specific surface area). In this way gas diffusion layer can be available for the reactions in order to minimize the transport resistance of the hydrogen and the oxygen in active layers. In addition, it can be interpreted as an easy removal of the water from the cathodic active layer and the minimum transport resistance of the protons from the active sites in the anodic layer to the active sites in the cathodic active layer.

Extensive researches have been proceeded to develop realistic simulation models in the past decade. Researchers all over the world are focusing on optimizing the fuel cell system to be cost competitive with currently available energy conversion devices [4].

Many studies have examined various aspects of PEMFC performance as a function of operating conditions (e.g.) [5–13]. One of the important tools in the optimization study of fuel cell performance is computational modeling, which can be used to reveal the fundamental phenomena that takes place in the fuel cell system [14].

A great number of researches have been conducted to improve the performance of the PEMFC, so that it can reach a significant market penetration. The performance of PEM fuel cells is influenced by many parameters, such as operating temperature, pressure, humidification of the gas streams and geometrical parameters. Among the various aspects of PEMFCs that affect cell performance, geometrical parameters play a major role. For example, performance of the fuel cell with smaller shoulder widths is better than those with larger ones [15–18].

Effect of gas channel geometry on the performance of proton exchange membrane fuel cells was developed to investigate its performance. Two geometries with rectangular and trapezoidal channel configuration were simulated and the results in a low cell voltage (which leads to high current densities in two geometries) are compared [19]. Ahmadi et al. investigated PEMFC performance in different cell potential [20]. Ahmadi et al. studied the effect of parallelogram gas channel and shoulder geometry on fuel cell performance [21] Also, Ahmadi, Rezazadeh, Mirzaee and Pourmahmoud investigated the effect of prominent Gas Diffusion Layers on PEMFC performance [22]. Ahmed and Sung performed simulations of PEMFCs with a new design for the channel shoulder geometry [23]. Grujicic and Chittajallu presented an optimized model for cathode geometry of PEMFCs [24].

In the present investigation, a three-dimensional, single phase, non-isothermal and parallel flow model of a PEM fuel cell with conventional and deflected membrane electrode assembly (MEA) that incorporates the key parameters affecting fuel cell performance has been simulated numerically. The humidified hydrogen was used on the anode side, and then air was applied on the cathode side. The available experimental data are used in order to validate the results of polarization curve. The studied model is modified and used to study the effects of reversing the cathode side gas flow on fuel cell characteristics. In this model, major transport phenomena of PEMFC was investigated carefully. The modeling data for base model was validated with experimental data.

## 2. MATHEMATICAL MODEL

In present study, computational domain and its grid are shown in Fig. 1. The cell consists of hydrogen and oxygen channels, bipolar plates on cathode and anode side of cell and membrane electrode assembly (MEA) is located between the gas channels.

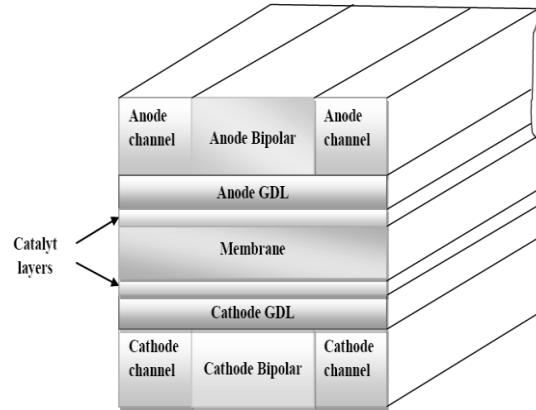


Fig. 1. Schematic of PEMFC (Computational domain)

### 3. MODEL ASSUMPTIONS

Present non iso-thermal model includes some assumptions as follows: All gases are assumed to be ideal gas mixture. GDLs and catalyst layers are homogeneous porous. The flow is incompressible and laminar, because the pressure gradients and velocities are small and volume of liquid-phase water in the domain is negligible. The flow field is single phase.

### 4. GOVERNING EQUATIONS

In this numerical simulation, a single domain model formation was used for the governing equations. These governing equations consist of mass conservation, momentum and species equations, which can be written as:

$$(\nabla \cdot \rho \mathbf{u}) = 0 \tag{1}$$

$$\frac{1}{(\varepsilon^{eff})^2} \nabla \cdot (\rho \mathbf{u} \mathbf{u}) = -\nabla P + \nabla \cdot (\mu \nabla \mathbf{u}) + S_u \tag{2}$$

$$\nabla \cdot (\mathbf{u} C_K) = \nabla \cdot (D_K^{eff} \nabla C_K) + S_K \tag{3}$$

$$\nabla \cdot (\kappa_e^{eff} \nabla \Phi_e) + S_\Phi = 0 \tag{4}$$

In Eq. (1)  $\rho$  is the density of gas mixture. According to model assumption, mass source and sink term are neglected. In the momentum equation (Eq. (2)) the effective porosity inside porous mediums and the viscosity of the gas mixture are shown by  $\varepsilon^{eff}$ ,  $\mu$  respectively. Darcy's drag for the flow which, through the porous gas diffusion layers and catalyst layers is explained by momentum source term ( $S_u$ ), as follows [25]:

$$S_u = -\frac{\mu}{K} \mathbf{u} \tag{5}$$

$K$  is the gas permeability inside porous mediums.  $D_K^{eff}$  is the effective diffusion coefficient of species  $k$  (e.g. hydrogen, oxygen, nitrogen and water vapor). It explains the effects of porosity in the porous gas diffusion and catalyst layers by the Bruggeman correlation[26]:

$$D_K^{eff} = (\varepsilon^{eff})^{1.5} D_K \tag{6}$$

Additionally, diffusion coefficient is a function of temperature and pressure [27] that is given by the next equation:

$$D_K = D_K^\circ \left( \frac{T}{T^\circ} \right)^{\frac{3}{2}} \left( \frac{P^\circ}{P} \right) \quad (7)$$

Transport properties for species are given in Table 1.

Table 1. Transport properties [27]

Property	value
H <sub>2</sub> Diffusivity in the gas channel, $D_{H_2}^0$	$1.10 \times 10^{-04} \text{ m}^2/\text{s}$
O <sub>2</sub> Diffusivity in the gas channel, $D_{O_2}^0$	$3.20 \times 10^{-05} \text{ m}^2/\text{s}$
H <sub>2</sub> O Diffusivity in the gas channel, $D_{H_2O}^0$	$7.35 \times 10^{-05} \text{ m}^2/\text{s}$
H <sub>2</sub> Diffusivity in the membrane, $D_{H_2}^{\text{mem}}$	$2.59 \times 10^{-10} \text{ m}^2/\text{s}$
O <sub>2</sub> Diffusivity in the membrane, $D_{O_2}^{\text{mem}}$	$1.22 \times 10^{-10} \text{ m}^2/\text{s}$

The charge conservation equation is shown as Eq. (4).  $\kappa_e$  is the ionic conductivity in the ion metric phase and has been incorporated by Springer, Zawodzinski and Gottesfeld [28]:

$$\kappa_e = \exp \left[ 1268 \left( \frac{1}{303} - \frac{1}{T} \right) \right] \times (0.005139\lambda - 0.00326) \quad (8)$$

Moreover, in the recent equation,  $\lambda$  is defined as the number of water molecules per sulfonate group inside the membrane. The water content can be assumed a function of water activity ( $a$ ). This parameter is defined through experimental data as follows [29]:

$$\lambda = 0.3 + 6a \left[ 1 - \tanh(a - 0.5) \right] + 3.9\sqrt{a} \left[ 1 + \tanh \left( \frac{a - 0.89}{0.23} \right) \right] \quad (9)$$

Water activity ( $a$ ) is defined by:

$$a = \frac{C_w RT}{P_w^{\text{sat}}} \quad (10)$$

The proton conductivity in the catalyst layers is defined by introducing the Bruggeman correlation [30]:

$$\kappa_e^{\text{eff}} = \varepsilon_m^{1.5} \kappa_e \quad (11)$$

In the above equation,  $\varepsilon_m$  is the volume fraction of the membrane-phase in the catalyst layer. The source and sink term in Eq. (3) and (4) are presented in Table 2. Local current density in the membrane can be calculated by:

$$I = -\kappa_e \nabla \Phi_e \quad (12)$$

Then the average current density is calculated as follows:

$$I_{\text{ave}} = \frac{1}{A} \int_{A_{\text{mem}}} I dA \quad (13)$$

where  $A$  is the active area over the MEA.

Table 2. Source/sink term for momentum, species and charge conservation equations for individual regions

	Momentum	species	charge
Flow channels	$S_u = 0$	$S_K = 0$	$S_\phi = 0$
Bipolar plates	$S_u = -\frac{\mu}{K} \mathbf{u}$	$S_K = 0$	$S_\phi = 0$
GDLs	$S_u = -\frac{\mu}{K} \mathbf{u}$	$S_K = 0$	$S_\phi = 0$
Catalyst layers	$S_u = 0$	$S_K = -\nabla \cdot \left( \frac{n_d}{F} \mathbf{i} \right) - \frac{S_K j}{nF}$	$S_\phi = j$
Membrane	$S_u = 0$	$S_K = -\nabla \cdot \left( \frac{n_d}{F} \mathbf{i} \right)$	$S_\phi = 0$

### 5. WATER TRANSPORT

Water molecules in PEM fuel cell are transported via electro-osmotic drag due to the properties of polymer electrolyte membrane and the molecular diffusion.  $H^+$  protons transport water molecules through the polymer electrolyte membrane. This transport phenomenon is called electro-osmotic drag. In addition to the molecular diffusion and electro-osmotic drag, water vapor is also produced in the catalyst layers due to the oxygen reduction reaction.

The water transport through the polymer electrolyte membrane is defined by:

$$\nabla \cdot (D_{H_2O}^{mem} \nabla C_{H_2O}^{mem}) - \nabla \cdot \left( \frac{n_d}{F} \mathbf{i} \right) = 0 \tag{14}$$

Where  $n_d$  and  $D_{H_2O}^{mem}$  are defined as the water drag coefficient from anode to cathode and the diffusion coefficient of water in the membrane phase, respectively.

The number of water molecules that are transported by each hydrogen proton  $H^+$  is called the water drag coefficient. It can be determined from the following equation [29]:

$$n_d = \begin{cases} 1 & \lambda < 9 \\ 0.117\lambda - 0.0544 & \lambda \geq 9 \end{cases} \tag{15}$$

The diffusion coefficient of water in the polymer membrane is dependent on the water content of the membrane and was developed by the following fits of the experimental expression [31]:

$$D_w^{mem} = \begin{cases} 3.1 \times 10^{-7} \lambda (e^{0.28\lambda} - 1) e^{\left(\frac{-2346}{T}\right)} & 0 < \lambda \leq 3 \\ 4.17 \times 10^{-8} (1 + 161e^{-\lambda}) e^{\left(\frac{-2346}{T}\right)} & \text{Otherwise} \end{cases} \tag{16}$$

Therefore the terms are function of the transfer current through the solid conductive materials and the membrane. The transfer currents or source terms are non-zero only inside the catalyst layers. The transfer current at anode and cathode is described by Tafel equations as follows:

$$R_{an} = j_{an}^{ref} \left( \frac{[H_2]}{[H_2]_{ref}} \right)^{\gamma_{an}} \left( e^{\alpha_{an} F \eta_{an} / RT} - e^{-\alpha_{ai} F \eta_{an} / RT} \right) \tag{17}$$

$$R_{cat} = j_{an}^{ref} \left( \frac{[O_2]}{[O_2]_{ref}} \right)^{\gamma_{cat}} \left( -e^{\alpha_{an} F \eta_{cat} / RT} + e^{-\alpha_{cat} F \eta_{cat} / RT} \right) \quad (18)$$

According to the Tafel equations, the current densities in the anode and cathode catalysts can be expressed by the exchange current density, reactant concentration, temperature and over-potentials that were defined through Tafel equations. Where, the surface over potential is defined as the difference between proton potential and electron potential.

$$\eta_{an} = \phi_{sol} - \phi_{mem} \quad (19)$$

$$\eta_{cat} = \phi_{sol} - \phi_{mem} - V_{oc} \quad (20)$$

The open circuit potential at the anode is assumed to be zero, while the open circuit potential at the cathode becomes a function of temperature as:

$$V_{oc} = 0.0025T + 0.2329 \quad (21)$$

The protonic conductivity of membrane is function of water content, where  $\sigma_m$  is the ionic conductivity in the ionomeric phase and has been correlated by Springer, Zawodinski and Gottesfeld. [32]:

$$\sigma_m = (0.005139\lambda - 0.00326) \exp \left[ 1268 \left( \frac{1}{303} - \frac{1}{T} \right) \right] \quad (22)$$

Energy equation is given by Eq. (23):

$$\nabla \cdot (\rho \mathbf{u} \mathbf{T}) = \nabla \cdot (\lambda_{eff} \nabla \mathbf{T}) + S_T \quad (23)$$

where  $\lambda_{eff}$  is the effective thermal conductivity, and the source term of the energy equation,  $S_T$ , is defined with the following equation:

$$S_T = I^2 R_{ohm} + h_{reaction} + \eta_a i_a + \eta_c i_c \quad (24)$$

In this equation,  $R_{ohm}$ , is the ohmic resistance of the membrane,  $h_{reaction}$ , is the heat generated through the chemical reactions.  $\eta_a$  and  $\eta_c$ , are the anode and cathode over potentials, which are calculated as follows:

$$R_{ohm} = \frac{t_m}{\sigma_e} \quad (25)$$

Here,  $t_m$  is the membrane thickness.

$$\eta_a = \frac{RT}{\alpha_a F} \ln \left[ \frac{IP}{j_{0_a} P_{0_{H_2}}} \right] \quad (26)$$

$$\eta_c = \frac{RT}{\alpha_c F} \ln \left[ \frac{IP}{j_{0_c} P_{0_{O_2}}} \right] \quad (27)$$

where  $\alpha_a$  and,  $\alpha_c$  are the anode and cathode transfer coefficients.  $P_{0_{H_2}}$ ,  $P_{0_{O_2}}$  are the partial pressure of hydrogen and oxygen respectively.  $j_0$  is the reference exchange current density. The fuel and oxidant fuel rate  $u$  is given by the following equations:

$$\mathbf{u}_{in,a} = \frac{\xi_a I_{ref} A_{mem}}{2C_{H_2,in} F A_{ch}} \quad (28)$$

$$\mathbf{u}_{in,c} = \frac{\xi_c I_{ref} A_{mem}}{4C_{O_2,in} F A_{ch}}$$

In the above equations,  $I_{ref}$  and  $\xi$  are the reference current density and stoichiometric ratio, respectively.  $\xi$  is defined as the ratio between the amount that is supplied and the amount that is required for the fuel, based on the reference current density. The species concentrations of flow inlets are assigned by the humidification conditions of both the anode and cathode inlets.

## 6. BOUNDARY CONDITION

Equations (1) through (4) form the complete set of governing equations in present mathematical model. Boundary conditions are dispensed at the external boundaries. Constant mass flow rate at the channel inlet and constant pressure condition at the channel outlet is considered. No-flux conditions are considered for mass, momentum, species and potential conservation equations on any boundaries except for inlets and outlets of the anode and cathode flow channels.

## 7. RESULTS AND DISCUSSION

### a) Model validation

A series of simulations were conducted from low to high operating current densities. In order to evaluate the validity of the model, numerical results (for parallel flow channels or base model) are compared with the experimental data presented by Wang, Husar, Zhou and Liu. [33]. As shown in Fig. 2, there is a good agreement between the results. The power density curve is illustrated for present model. As we know, there is a relation between voltage, current density and the power of the fuel cell as  $P=V \times I$ . Then the main goal of this research is simulation of this parameter in the fuel cells with counter flow channels. The important results in this research are highlighted.

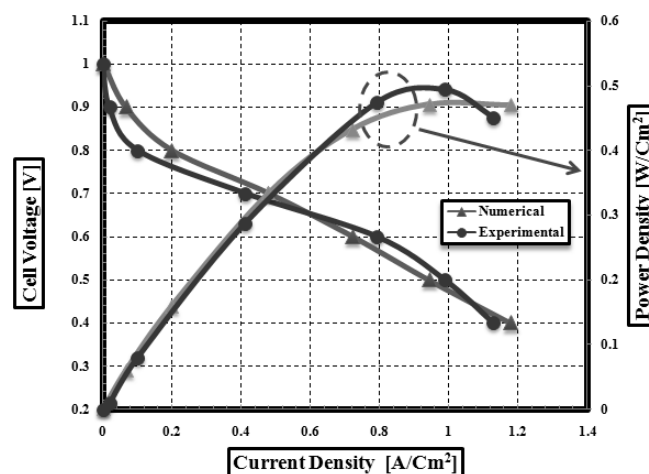


Fig. 2. Polarization and power density curve

The operating conditions of the fuel cell and geometric parameters are shown in Table 3. They are used for fully humidified inlet condition for anode and cathode. The transfer current at anode and cathode can be described by Tafel equations.

Table 3. Geometrical parameters and operating conditions [33]

Parameter	value
Gas channel length	$4.0 \times 10^{-2}$ m
Gas channel width and depth	$0.762 \times 10^{-3}$ m
Bipolar plate width	$1.524 \times 10^{-3}$ m
Gas diffusion layer thickness	$2.54 \times 10^{-4}$ m
Catalyst layer thickness	$2.87 \times 10^{-5}$ m
Membrane thickness	$4.023 \times 10^{-4}$ m
Cell temperature	80 <sup>0</sup> C
Anode pressure	1 atm
Cathode pressure	1 atm

In this article the new model with counter flow channels is chosen to compare with the base model (fuel cell with the parallel flow channels). All the geometrical parameters and operating conditions are the same in both models. The computational mesh structure is divided into 50000 cells; also the inlet and outlet sections of gas channels (at the anode and cathode side) are presented in Fig. 3. Figure 4 compares polarization curve of two numerical cases (parallel flow and counter flow). Numerical results show that the system with the parallel flow channels produces more current density in comparison with the model with counter flow channels, at the same cell voltage.

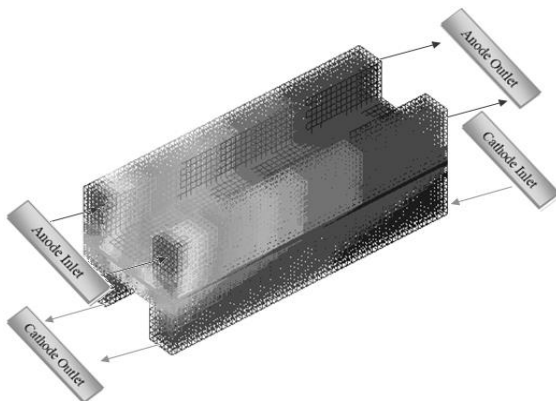


Fig. 3. Grid of Computational Domain

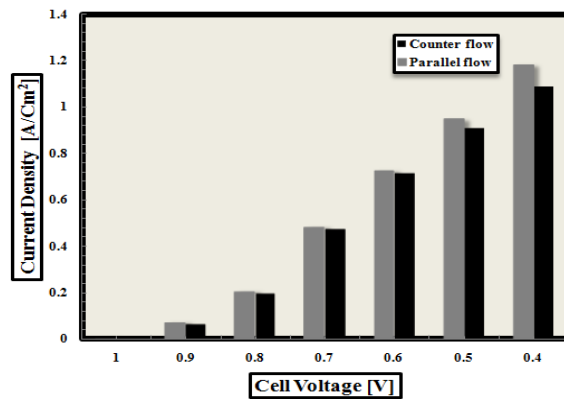


Fig. 4. Polarization Curve of two numerical models

Figures 5 and 6 specify temperature distribution of counter flow PEM fuel cell for two different voltages (0.7 V, 0.5V).As these figures show, the maximum temperature magnitude in the voltage 0.5V is more than maximum temperature magnitude at 0.7 V. This is due to high reaction rate in fuel cell at lower voltages. Voltage gradually decreases with increasing reaction rate and maximum cell temperature reduces.

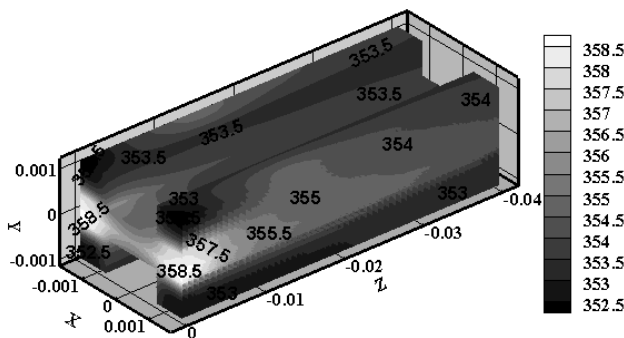


Fig. 5. Temperature Distribution at 0.5 Volt (K)

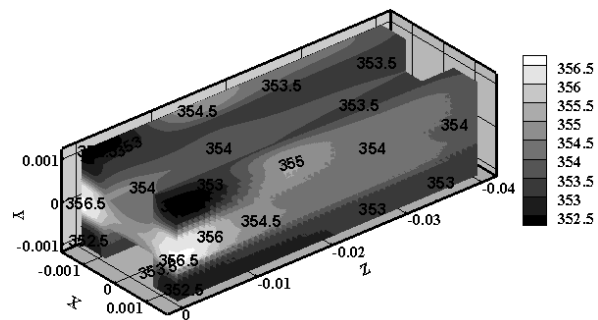


Fig. 6. Temperature Distribution at 0.7 Volt (K)

Species distribution and water transport management in the base model is acceptable physically. The water distribution at the anode and cathode sides has a balanced form. It means that if the water concentration along the anode side is reduced, because of transporting hydrogen protons to the electro chemical reaction area at the cathode side, it should increase due to combination of oxygen molecules and electrons and hydrogen protons. But in the new case, by reversing the flow direction of the cathode side, water accumulation in the exit region of the cathode side (entry region of anode side). Figures 7 and 8 indicate the previous explanation about the water distribution schematically.

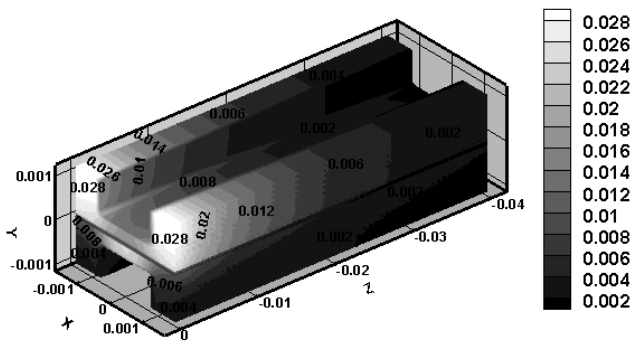


Fig. 7. Water Concentration at 0.5 Volt ( $\text{Kmol/m}^3$ )

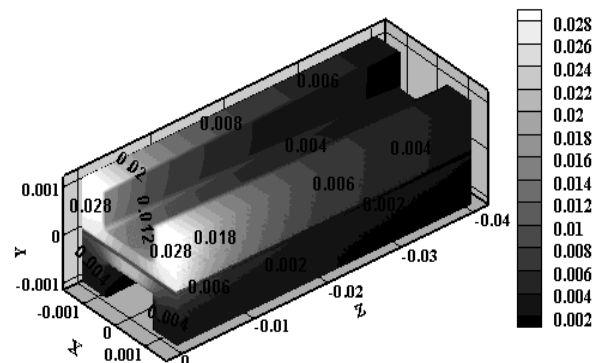


Fig. 8. Water Concentration at 0.7 Volt ( $\text{Kmol/m}^3$ )

It is clear that at the cathode side, where the main electro chemical reaction occurs, the amount of oxygen should be decreased because of its consumption. By reversing cathode flow direction, the minimum oxygen magnitude at the end part of cathode channel encounters the maximum hydrogen protons amount. This fact results in fuel cell performance reduction (Figs. 9, 12).

Activation over potential and current density at the cathode catalyst layer surface is presented in Figs. 10, 11, 13 and 14 for two different cell voltages. At the cathode side, oxygen, current density and over-potential are low at the entry region of gas flow channel and then increase along the channel, as shown in the figures. As is shown in Figs. 10 and 13 the over-potential values are negative. In most references it appears with positive values, so in figures the over-potential contour is presented by positive range. In this way, at the entry region of the cathode catalyst layer the over-potential reaches its minimum magnitudes (or reaches to its maximum magnitudes at the exit regions). The contour of current density is found to correlate with oxygen and activation over-potential contour. Figures 15 and 16 compare oxygen and water concentration for two cell voltages at the catalyst layers along the channel. It is observed that the oxygen consumed along the channel at the flow direction is due to chemical reaction. Water transport through the membrane is one of critical parameter which determines membrane water content and fuel cell performance. The water molecules diffuse through the membrane from anode to the cathode due to Electro-osmotic drag to react with oxygen and the returning electron, therefore water is successively produced at the cathode. Part of the water will return back from cathode to the anode through back-diffusion. Electro-osmotic mass and back diffusion flux across the membrane are compared in Figs. 17, 18 for two voltages.

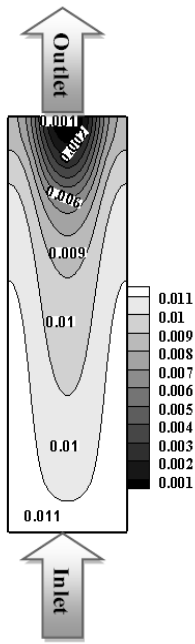


Fig. 9. Oxygen Concentration at 0.5 Volt at the interface of Cathode Catalyst and Membrane (Kmol/m<sup>3</sup>)

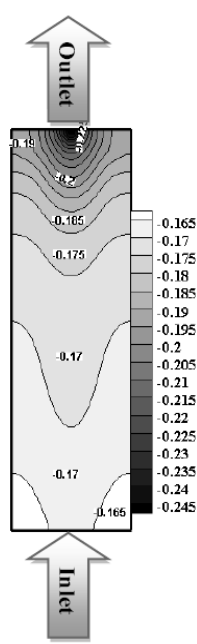


Fig. 10. Over-potential Distribution at 0.5 Volt at the interface of Cathode Catalyst and Membrane (Volt)

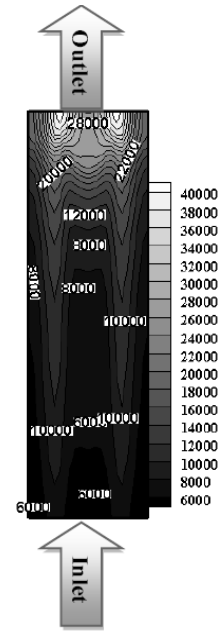


Fig. 11. Current Flux Density at 0.5 Volt at the interface of Cathode Catalyst and Membrane (amp/m<sup>2</sup>)

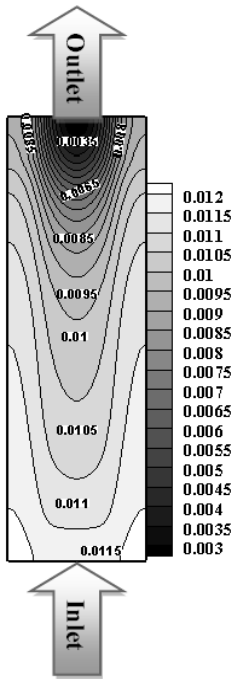


Fig. 12. Oxygen Concentration at 0.7 Volt at the interface of Cathode Catalyst and Membrane (Kmol/m<sup>3</sup>)

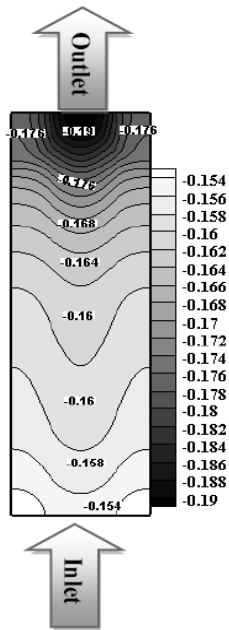


Fig. 13. Over-potential Distribution at 0.7 Volt at the interface of Cathode Catalyst and Membrane (Volt)

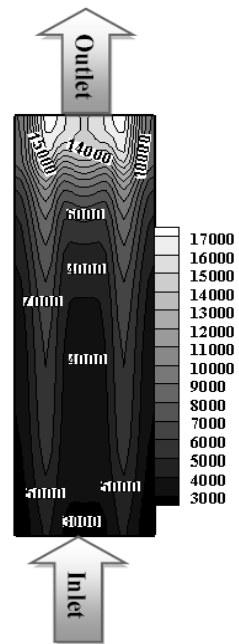


Fig. 14. Current Flux Density at 0.7 Volt at the interface of Cathode Catalyst and Membrane (amp/m<sup>2</sup>)

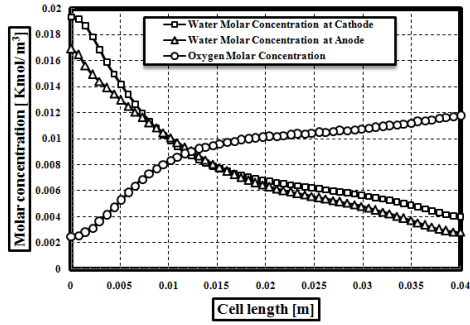


Fig. 15. Oxygen and Water Concentration at 0.5 Volt at the interface of Cathode Catalyst and Membrane ( $\text{Kmol/m}^3$ )

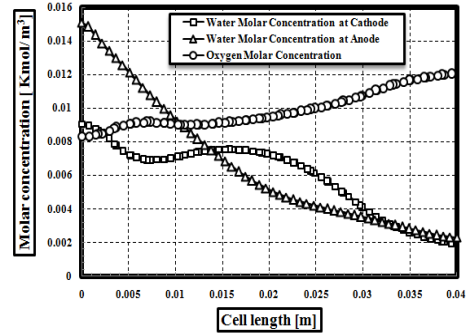


Fig. 16. Oxygen and Water Concentration at 0.7 Volt at the interface of Cathode Catalyst and Membrane ( $\text{Kmol/m}^3$ )

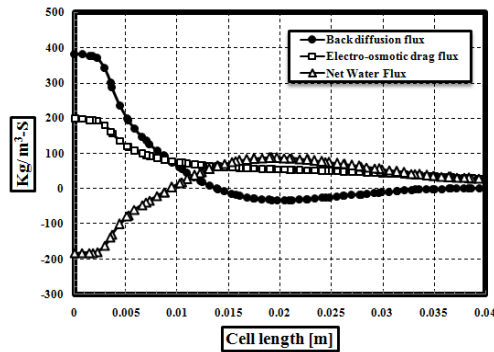


Fig. 17. Water Flux Comparison at 0.5 Volt at the interface of Cathode Catalyst and Membrane ( $\text{Kg/m}^3\text{-S}$ )

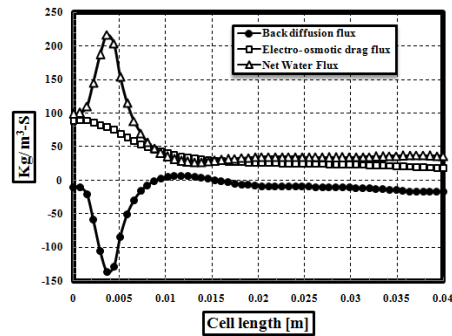


Fig. 18. Water Flux Comparison at 0.7 Volt at the interface of Cathode Catalyst and Membrane ( $\text{Kg/m}^3\text{-S}$ )

The net water flux passing the membrane layer is equal to subtracting the magnitude of back diffusion flux from electro-osmotic mass flux. Figures 19 through 22 show the current density distribution along the channel at the interface of membrane and cathode catalyst layer for four different voltages. It is observed that, because of low electro-chemical reaction rate at 1.0 V, the current density at this voltage has the minimum value. The current density at the inlet was the lowest and increased along the channel due to reversing the flow direction at cathode side. The lowest value of current density is probably at inlet region of cathode side because of the low concentration of hydrogen proton to react with oxygen and low electro-osmotic mass flux at the inlet region.

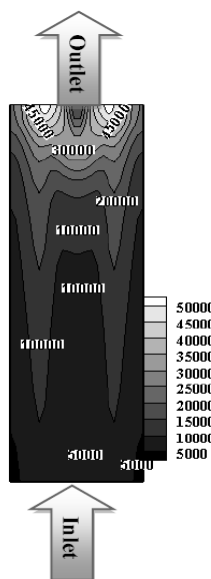


Fig. 19. Current Flux Density at 0.4 Volt at the interface of Cathode Catalyst and Membrane ( $\text{amp/m}^2$ )

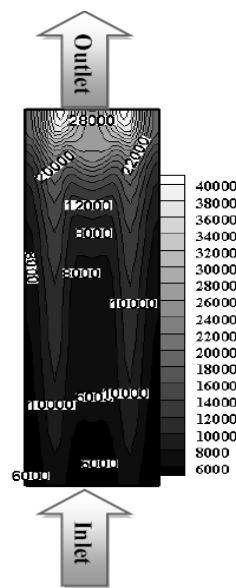


Fig. 20. Current Flux Density at 0.5 Volt at the interface of Cathode Catalyst and Membrane ( $\text{amp/m}^2$ )

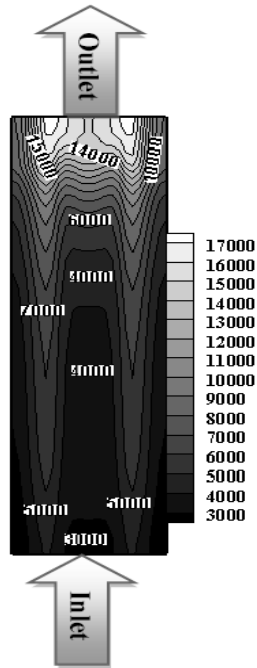


Fig. 21. Current Flux Density at 0.7Volt at the interface of Cathode Catalyst and Membrane (amp/m<sup>2</sup>)

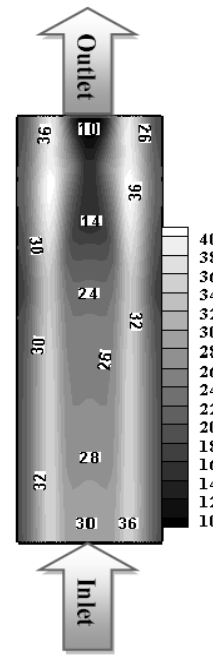


Fig. 22. Current Flux Density at 1Volt at the interface of Cathode Catalyst and Membrane (amp/m<sup>2</sup>)

## 8. CONCLUSION

- In present study, a three dimensional, computational fluid dynamic model of a conventional PEM fuel cell with straight flow channels was developed for the base model.
- In order to investigate the effect of reversing the flow direction on cell performance, the flow direction at the cathode gas channel is reversed and studied numerically. The polarization, power density, oxygen and water concentration curves in the cathode and anode, extracted from numerical results clearly indicated good agreement between numerical results and experimental data (for the base model).
- The transport phenomena such as species concentration curves and contours, over-potential, current density distribution, and electro-osmotic mass and back diffusion flux across the membrane were compared. The results showed that by reversing the flow direction at cathode side the species and current density distribution are changed subsequently, which causes the water accumulation in the exit region of the cathode side.
- The water molecules diffuse through the membrane from the anode to the cathode due to Electro-osmotic drag to react with oxygen and the returning electron, therefore water is successively produced at the cathode. Part of the water will return back from the cathode to the anode through back-diffusion.
- The other effect of reversing the flow direction is the minimum oxygen magnitude at the end part of cathode channel encounters the maximum hydrogen protons amount which results in the fuel cell performance reduction significantly. The current density at the inlet was the lowest and increased along the channel due to reversing the flow direction at cathode side. The lowest value of current density is probably at the inlet region of cathode side because of the low concentration of hydrogen proton to react with oxygen and low electro-osmotic mass flux at the inlet region.

**Acknowledgment:** This research was sponsored by Renewable Energy Organization of Iran.

## NOMENCLATURE

$a$	water activity	$\mu$	viscosity (kg/m-s)
$C$	molar concentration (mol/m <sup>3</sup> )	$\sigma_e$	membrane conductivity (1/ohm-m)
$D$	mass diffusion coefficient (m <sup>2</sup> /s)	$\lambda$	water content in the membrane
$F$	faraday constant (C/mol)	$\zeta$	stoichiometric ratio
$I$	local current density (A/m <sup>2</sup> )	$\eta$	over potential (v)
$J$	exchange current density (A/m <sup>2</sup> )	$\lambda_{eff}$	effective thermal conductivity (w/m-k)
$K$	permeability (m <sup>2</sup> )		
$M$	molecular weight (kg/mol)		
$n_d$	electro-osmotic drag coefficient		
$P$	pressure (Pa)		
$R$	universal gas constant (J/mol-K)		
$T$	temperature (K)		
$t$	thickness		
$\vec{u}$	velocity vector		
$V_{cell}$	cell voltage		
$V_{oc}$	Open-circuit voltage		
$W$	width		
$X$	mole fraction		
<b>Greek letters</b>			
$\alpha$	water transfer coefficient		
$\varepsilon^{eff}$	effective porosity		
$\rho$	density (kg/m <sup>3</sup> )		
$\phi_e$	electrolyte phase potential (v)		
<b>Subscripts and superscripts</b>			
a	anode		
c	cathode		
ch	channel		
k	chemical species		
m	membrane		
MEA	membrane electrolyte assembly		
ref	reference value		
sat	saturated		
w	water		

## REFERENCES

1. Kazim, A., Liu, H.T. & Forges, P. (1999). Modeling of performance of PEM fuel cells with conventional and interdigitated flow fields. *J. Appl. Electrochem.*, Vol. 29, pp. 1409–1416.
2. Nguyen, T. V. (1999). Modeling two-phase flow in the porous electrodes of proton exchange membrane fuel cells using the interdigitated flow fields. *Presented at the 195th Meeting of Electrochemical Society*, Seattle.
3. Wood, D. L., Yi, J. S. & Nguyen, T. V. (1998). Effect of direct liquid water injection and interdigitated flow field on the performance of proton exchange membrane fuel cells. *Electrochem.* Vol. 43, pp. 3795–3809.
4. Grujicic, M. & Chittajallu, K. M. (2004). Design and optimization of polymer electrolyte membrane (PEM) fuel cells. *Applied Surface Science*, Vol. 227, pp. 56–72.
5. Xing et al. (2010). Optimization of assembly clamping pressure on performance of proton-exchange membrane fuel cells. *J. Power Sources*, Vol. 195, pp. 62-68.
6. Chang, et al. (2007). Effect of clamping pressure on the performance on a PEM fuel cell. *J. Power Sources*, Vol. 166, pp. 149-154.
7. Rho, Y. W., Velev, O. A., Srinivasan, S. & Kho, Y. T. (1994). Mass transport in proton exchange membrane fuel cells using O<sub>2</sub>/H<sub>2</sub>, O<sub>2</sub>/Ar, and O<sub>2</sub>/N<sub>2</sub> mixtures. *J. Electrochem. Soc.*, Vol. 141, pp. 2089–2096.
8. Amphlett, J. C., Baumert, R. M., Mann, R. F., Peppley, B. A., Roberge, P. R. & Harris, T. J. (1995). Performance modeling of the Ballard Mark IV solid polymer electrolyte fuel cell. I. Mechanistic model development. *J. Electrochem. Soc.*, Vol. 142, pp. 9-15.
9. Mosdale, R. & Srinivasan, S. (1995). Analysis of performance and of water management in proton exchange membrane fuel cells. *Electrochem. Acta*, Vol. 40, pp. 413-421.
10. Oetjen, H. F., Schmidt, V. M., Stimming, U. & Trila, F. (1996). Performance data of a proton exchange membrane fuel cell using H<sub>2</sub>/Co as fuel gas. *J. Electrochem. Soc.*, Vol. 143, pp. 3838-3842.

11. Büchi, F. N. & Srinivasan, D. (1997). Operating proton exchange membrane fuel cells without external humidification of the reactant gases. *J. Electrochem. Soc.*, Vol. 144, pp. 2767-2772.
12. Uribe, F. A., Gottesfeld, S. & Zawodzinski, T. A. (2002). Effect of ammonia as potential fuel impurity on proton exchange membrane fuel cell performance. *J. Electrochem. Soc.*, Vol. 149, pp. A293-A296.
13. Ticianelli, E. A., Derouin, C. R. & Srinivasan, S. (1988). Localization of platinum in low catalyst loading electrodes to attain high power densities in SPE fuel cells. *J. Electroanal. Chem.*, Vol. 251, pp. 275–295.
14. Yao, K. Z., Karan, K., McAuley, K. B., Oosthuizen, P., Peppley, B. & Xie, T. (2004). A review of mathematical models for hydrogen and direct methanol polymer electrolyte membrane fuel cells. *Fuel Cells*, Vol. 4, No. ½, pp. 3–29.
15. Natarajan, D. & Nguyen, T. V. (2001). A two-dimensional, two-phase, multi component, transient model for the cathode of a proton exchange membrane fuel cell using conventional gas distributors. *J. Electrochem.Soc.*, Vol. 148, No. 12, pp. A1324–A1335.
16. Lin, G. & Nguyen, T. V. (2006). A two-dimensional two-phase model of a PEM fuel cell. *J. Electrochem. Soc.*, Vol. 153, pp. A372–A382.
17. Lum, K. W. & McGuirk, J. J. (2005). Three-dimensional model of a complete polymer electrolyte membrane fuel cell – model formulation, validation and parametric studies. *J. Power Source*, Vol. 143, pp. 103–124.
18. Ahmed, D. H. & Sung, H. J. (2006). Effects of channel geometrical configuration and shoulder width on PEMFC performance at high current density. *J. Power Source*. Vol. 162, pp. 327–339.
19. Majidifar, S., Mirzaei, I., Rezazadeh, S., Mohajeri, P. & Oryani, H. (2011). Effect of gas channel geometry on performance of PEM fuel cells. *AJBAS*, Vol. 5, No. 5, pp. 943-954.
20. Ahmadi, N., Pourmahmoud, N., Mirzaee, I. & Rezazadeh, S. (2012). Three-dimensional computational fluid dynamic study on performance of polymer exchange membrane fuel cell (PEMFC) in different cell potential. *Iranian Journal of Science & Technology, Transactions of Mechanical Engineering*, Vol. 36, No. 2, pp. 129-141.
21. Ahmadi, N., Pourmahmoud, N., Mirzaee, I. & Rezazadeh, S. (2011). Three-dimensional computational fluid dynamic study of effect of different channel and shoulder geometries on cell performance. *AJBAS*, Vol. 5, No. 12, pp. 541-556.
22. Ahmadi, N., Rezazadeh, S., Mirzaee, I. & Pourmahmoud, N. (2012). Three-dimensional computational fluid dynamic analysis of the conventional PEM fuel cell and investigation of prominent gas diffusion layers effect. *JMST*, Vol. 26, No. 8, pp. 1-11.
23. Ahmed, D. H. & Sung, H. J. (2008). Design of a deflected membrane electrode assembly for PEMFCs. *Int. J. Heat and Mass Transfer*, Vol. 51, pp. 5443–5453.
24. Grujicic, M. & Chittajallu, K. M. (2004). Design and optimization of the Cathode Geometry in polymer electrolyte membrane (PEM) fuel cells. *Chemical Engineering Science*, Vol. 59, pp. 5883-5895.
25. Garau, V., Liu, H. & Kakac, S. (1998). Two-dimensional model for proton exchange membrane fuel cells. *AIChE J.*, Vol. 44, No. 11, pp. 2410-2422.
26. Meredith, R. E. & Tobias, C. W. (1960). *Advances in electrochemistry and electrochemical engineering 2*. Tobias,C.W., ed., Interscience Publishers, New York.
27. Byron Bird, R., Stewart, W. E. & Lightfoot, E. N. (1960). *Transport phenomena*, John Wiley & Sons, Inc.
28. Springer, T. E., Zawodzinski, T. A. & Gottesfeld, S. (1991). Polymer electrolyte fuel cell model. *J. Electrochem. Soc.*, Vol. 138, pp. 2334-2342.
29. Kuklikovsky, A. A. (2003). Quasi-3D modeling of water transport in polymer electrolyte fuel cells. *J. Electrochem. Soc.*, Vol. 150, No. 11, pp. A1432-A1439.
30. Meredith, R. E. & Tobias, C. W. (1960). *Advances in electrochemistry and electrochemical engineering 2*. Tobias, C.W., ed., Interscience Publishers, New York.

31. Yeo, S. W. & Eisenberg, A. (1977). Physical properties and supermolecular structure of perfluorinated ion-containing (nafion) polymers, *J. Appl. Polym. Sci.*, Vol. 21, pp. 875-898.
32. Springer, T. E., Zawodinski, T. A. & Gottesfeld, S. (1991). Polymer electrolyte fuel cell model, *J. Electrochem. Soc.*, Vol. 136, pp. 2334-2342.
33. Wang, L., Husar, A., Zhou, T. & Liu, H. (2003). A parameteric study of PEM fuel cell performances, *J. Hydrog. Energy*, Vol. 28, pp. 1263-1272.